VI International Conference on Computational Methods for Coupled Problems in Science and Engineering
COUPLED PROBLEMS 2015
B. Schrefler, E. Oñate and M. Papadrakakis (Eds)

HYBRID SIMULATION OF COMPLEX STRUCTURAL SYSTEMS BASED ON PARTITIONED TIME INTEGRATION SCHEMES

Giuseppe Abbiati*, Enrico Cazzador†, Oreste S. Bursi†, Pierre Pegon~, Francisco Javier Molina~ and Fabrizio Paolacci§.

* Department of Civil, Environmental and Geomatic Engineering (D-BAUG), IBK, ETH Zurich
Stefano-Franscini-Platz 5, 8093 Zürich, Switzerland
e-mail: abbiati@ibk.baug.ethz.ch

† Department of Civil, Environmental and Mechanical Engineering, University of Trento
Via Mesiano 77, 38123, Trento, Italy
e-mail: oreste.bursi@unitn.it, enrico.cazzador@unitn.it

§ Department of Engineering, University of Roma Tre
Via Vito Volterra 62, Rome, Italy
e-mail: fabrizio.paolacci@uniroma3.it

~ European Commission, Joint Research Centre (JRC), Institute for the Protection and Security of the Citizen,
European Laboratory for Structural Assessment Unit, Via Enrico Fermi 2749, 21027 Ispra (VA), Italy
e-mail: pierre.pegon@jrc.ec.europa.eu

Key words: Hybrid Simulations, Finite element, Partitioned algorithms, Structural dynamics, Reinforced concrete old viaduct.

Abstract. In the last two decades, the increasing complexity of engineering systems boosted the development of very efficient simulation methods based on partitioning. In view of coupling dynamic parts of hybrid systems, the finite element tearing and interconnecting approach emerged as the most promising technique. Nonetheless, there is still a lack of a comprehensive study of algorithmic performances from the experimental perspective. In this view, the present paper sheds light on the application of two well-known parallel partitioning methods for the purpose of the simulation of hybrid models. Thus, an existent reinforced concrete bridge is chosen as a benchmark case study. In order to perform hybrid simulations, a novel coupling software was devised. It allowed for combining two physical piers to the numerical model of the remaining part of the bridge. As a result, successful tests were conducted at the ELSA laboratory of the Joint Research Centre of Ispra (Italy).

1 INTRODUCTION

In view of coupling dynamic parts of hybrid systems, partitioning methods are more than ever appealing and arouse a lot of interest in the context of hybrid experimental/numerical simulation techniques [1]. In fact, they are prone to combine a Physical Substructure (PS), which is the key region of interest of the emulated heterogeneous system, and a Numerical Substructure (NS) collecting all well-known subparts. During a heterogeneous simulation, a compliant time integrator calculates the interaction between NS and PS by solving the equation of motion of the entire system. Since Finite Element Tearing and Interconnecting (FETI) approaches allow for the concurrent solution of involved subdomains with large time step ratios, they guarantiee

a smooth stream of displacement commands on the PS, regardless the coarser time grid on the NS. In this context, [2] proved that velocity continuity on interface DoFs is the key solution to obtain unconditionally stable algorithms as long as all individual subdomains satisfy their own stability requirements. Along this line, Pegon and Magonette developed the PM method [3], which paved the way for parallel implementations of the FETI tailored to hybrid models. Interface energy dissipation and one order of accuracy loss in the subcycling case were stressed as major drawbacks. Moreover, the PM method needs for a starting procedure. Brun et al. proposed an improved variant of the PH algorithm [4], namely the modified PH method [5], which allows for computations in subdomains in a completely concurrent manner with no need for initialization and energy conserving.

Mixed implicit/explicit multi-time partitioning methods tailored to Newmark schemes are ripe for a profitable application to hybrid simulations. Nevertheless, there is still a lack of a comprehensive study of algorithmic performances from an experimental perspective. Along this line, this paper presents algorithmic implementations of both the PM and modified PH methods tailored to both numerical/physical nonlinear systems. A twelve-pier reinforced concrete bridge is introduced as reference case study. Then, numerical simulations of the dynamic response of the bridge emphasize pros and cons of both algorithms. Finally, the experimental implementation of the PM method, which allows for conducting hybrid simulations of aforementioned bridge at the ELSA Laboratory of the Joint Research Centre of Ispra (Italy) is presented.

2 PARTITIONED INTEGRATORS FOR SUBDOMAIN COUPLING IN HYBRID SIMULATIONS

Both the PM and the modified PH algorithms are presented in this section. In detail, all implementations refer to the following set of coupled of nonlinear dynamic equations,

$$\begin{cases} \mathbf{M}^A\ddot{\mathbf{u}}^A + \mathbf{R}^A\left(\mathbf{u}^A, \dot{\mathbf{u}}^A\right) + \mathbf{L}^{A^T}\boldsymbol{\Lambda} = \mathbf{F}^A\left(t\right) \\ \mathbf{M}^B\ddot{\mathbf{u}}^B + \mathbf{R}^B\left(\mathbf{u}^B, \dot{\mathbf{u}}^B\right) + \mathbf{L}^{B^T}\boldsymbol{\Lambda} = \mathbf{F}^B\left(t\right) \end{cases} \tag{1}$$

$$\mathbf{L}^A\dot{\mathbf{u}}^A + \mathbf{L}^B\dot{\mathbf{u}}^B = \mathbf{0} \tag{2}$$

where, with regard to the generic subdomain k, $\mathbf{M}^k$ is the mass matrix; $\mathbf{u}^k, \dot{\mathbf{u}}^k$ and $\ddot{\mathbf{u}}^k$ are displacement, velocity and acceleration vectors, $\mathbf{R}^k$ is the restoring force and $\mathbf{F}^k(t)$ represents the external time-varying load. $\mathbf{L}^k$ is a Boolean matrix that collocates interface DoFs on the related subdomain. According to [2], in order to obtain unconditionally stable algorithms as long as all individual subdomains satisfy their own stability requirements, velocity continuity on interface DoFs is pursued. For the sake of clarity, zero tangent stiffness $\mathbf{K}^k$ and damping $\mathbf{C}^k$matrices read,

$$\mathbf{K}^k = \left.\frac{\partial \mathbf{R}^k}{\partial \mathbf{u}^k}\right|_{\mathbf{u}^k, \dot{\mathbf{u}}^k = \mathbf{0}}, \mathbf{C}^k = \left.\frac{\partial \mathbf{R}^k}{\partial \dot{\mathbf{u}}^k}\right|_{\mathbf{u}^k, \dot{\mathbf{u}}^k = \mathbf{0}} \tag{3}$$

Both coupling method are supposed to handle a pair of arbitrary Newmark schemes with their own characteristic parameters, i.e. β_A, γ_A, and β_B, γ_B, for subdomains A and B, respectively [6].

2.1 The PM method

The task sequence of the PM method, analyzed in depth in [7] is sketched in Figure 1. It clearly recalls the GC method [2].However, a time step equal to $2\Delta t_A$ is exploited in subdomain A in order to anticipate information on the subdomain B at the beginning of a new time step t_{n+1}.

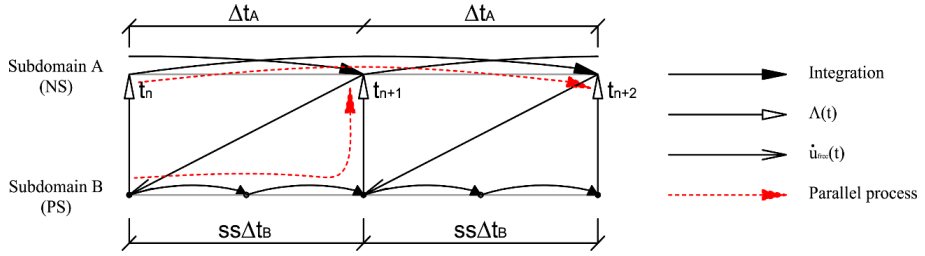

Fig. 1 - Task sequence of the PM method algorithm.

The dashed line describes the ongoing parallel process in the two subdomains. Note that the synchronized exchange of information enables the parallel computation of both subdomains. The PM method is briefly summarized hereinafter.

Subdomain A

if n == 1

Initialization step on subdomain A from $\boldsymbol{t_n}$ to $\boldsymbol{t_{n+1}}$

$$\tilde{\mathbf{u}}_{n+1}^{A,free} = \mathbf{u}_n^A + \dot{\mathbf{u}}_n^A \Delta t^A + \ddot{\mathbf{u}}_n^A \left(1/2 - \beta^A\right)\left(\Delta t^A\right)^2$$

$$\tilde{\dot{\mathbf{u}}}_{n+1}^{A,free} = \dot{\mathbf{u}}_n^A + \ddot{\mathbf{u}}_n^A \left(1-\gamma^A\right)\left(\Delta t^A\right)$$

$$\ddot{\mathbf{u}}_{n+1}^{A,free} = \mathbf{D}_1^{A^{-1}}\left(\mathbf{F}_{n+1}^A - \mathbf{R}^A\left(\tilde{\mathbf{u}}_{n+1}^{A,free}, \tilde{\dot{\mathbf{u}}}_{n+1}^{A,free}\right)\right)$$

$$\dot{\mathbf{u}}_{n+1}^{A,free} = \tilde{\dot{\mathbf{u}}}_{n+1}^{A,free} + \ddot{\mathbf{u}}_{n+1}^{A,free}\gamma^A\left(\Delta t^A\right)$$

$$\mathbf{u}_{n+1}^{A,free} = \tilde{\mathbf{u}}_{n+1}^{A,free} + \ddot{\mathbf{u}}_{n+1}^{A,free}\beta^A\left(\Delta t^A\right)^2$$

end

Solution of the free problem on subdomain A from $\boldsymbol{t_n}$ to $\boldsymbol{t_{n+2}}$

$$\tilde{\mathbf{u}}_{n+2}^{A,free} = \mathbf{u}_n^A + \dot{\mathbf{u}}_n^A 2\Delta t^A + \ddot{\mathbf{u}}_n^A \left(1/2 - \beta^A\right)\left(2\Delta t^A\right)^2$$

$$\tilde{\dot{\mathbf{u}}}_{n+2}^{A,free} = \dot{\mathbf{u}}_n^A + \ddot{\mathbf{u}}_n^A \left(1-\gamma^A\right)\left(2\Delta t^A\right)$$

$$\ddot{\mathbf{u}}_{n+2}^{A,free} = \mathbf{D}_2^{A^{-1}}\left(\mathbf{F}_{n+2}^A - \mathbf{R}^A\left(\tilde{\mathbf{u}}_{n+2}^{A,free}, \tilde{\dot{\mathbf{u}}}_{n+2}^{A,free}\right)\right)$$

Subdomain B

for = j 1:1:ss

Solution of the free problem on subdomain B from $\boldsymbol{t_{n+\frac{j-1}{ss}}}$ to $\boldsymbol{t_{n+\frac{j}{ss}}}$

$$\tilde{\mathbf{u}}_{n+\frac{j}{ss}}^{B,free} = \mathbf{u}_{n+\frac{j-1}{ss}}^B + \dot{\mathbf{u}}_{n+\frac{j-1}{ss}}^B \Delta t^B + \ddot{\mathbf{u}}_{n+\frac{j-1}{ss}}^B \left(1/2 - \beta^B\right)\Delta t^{B^2}$$

$$\tilde{\dot{\mathbf{u}}}_{n+\frac{j}{ss}}^{B,free} = \dot{\mathbf{u}}_{n+\frac{j-1}{ss}}^B + \ddot{\mathbf{u}}_{n+\frac{j-1}{ss}}^B \left(1-\gamma^B\right)\Delta t^B$$

$$\ddot{\mathbf{u}}_{n+\frac{j}{ss}}^{B,free} = \mathbf{D}^{B^{-1}}\left(\mathbf{F}_{n+\frac{j}{ss}}^B - \mathbf{R}^B\left(\tilde{\mathbf{u}}_{n+\frac{j}{ss}}^{B,free}, \tilde{\dot{\mathbf{u}}}_{n+\frac{j}{ss}}^{B,free}\right)\right)$$

$$\dot{\mathbf{u}}_{n+\frac{j}{ss}}^{B,free} = \tilde{\dot{\mathbf{u}}}_{n+\frac{j}{ss}}^{B,free} + \ddot{\mathbf{u}}_{n+\frac{j}{ss}}^{B,free}\gamma^B\Delta t^B$$

$$\mathbf{u}_{n+\frac{j}{ss}}^{B,free} = \tilde{\mathbf{u}}_{n+\frac{j}{ss}}^{B,free} + \ddot{\mathbf{u}}_{n+\frac{j}{ss}}^{B,free}\beta^B\Delta t^{B^2}$$

Interpolation of free quantities on subdomain A

$$\dot{\mathbf{u}}_{n+\frac{j}{ss}}^{A,free} = \left(1-\frac{j}{ss}\right)\dot{\mathbf{u}}_n^{A,free} + \left(\frac{j}{ss}\right)\dot{\mathbf{u}}_{n+1}^{A,free}$$

Calculation of interface Lagrange multipliers

$$\boldsymbol{\Lambda}_{n+\frac{j}{ss}} = \mathbf{H}^{AB^{-1}}\left(\mathbf{L}^A\dot{\mathbf{u}}_{n+\frac{j}{ss}}^{A,free} + \mathbf{L}^B\dot{\mathbf{u}}_{n+\frac{j}{ss}}^{B,free}\right)$$

Solution of the link problem on subdomain B

$$\ddot{\mathbf{u}}_{n+\frac{j}{ss}}^{B,link} = -\mathbf{D}^{B^{-1}}\mathbf{L}^{B^T}\boldsymbol{\Lambda}_{n+\frac{j}{ss}}$$

$$\dot{\mathbf{u}}_{n+2}^{A,\,free} = \dot{\tilde{\mathbf{u}}}_{n+2}^{A,\,free} + \ddot{\mathbf{u}}_{n+2}^{A,\,free}\gamma^{A}\left(2\Delta t^{A}\right)$$

$$\mathbf{u}_{n+2}^{A,\,free} = \tilde{\mathbf{u}}_{n+2}^{A,\,free} + \ddot{\mathbf{u}}_{n+2}^{A,\,free}\beta^{A}\left(2\Delta t^{A}\right)^{2}$$

Solution of the link problem on subdomain A

$$\ddot{\mathbf{u}}_{n+1}^{A,link} = -\mathbf{D}_{m}^{A^{-1}}\mathbf{L}^{A^{T}}\boldsymbol{\Lambda}_{n+1}$$

$$\dot{\mathbf{u}}_{n+1}^{A,link} = \ddot{\mathbf{u}}_{n+1}^{A,link}\gamma^{A}\left(m\Delta t^{A}\right)$$

$$\mathbf{u}_{n+1}^{A,link} = \ddot{\mathbf{u}}_{n+1}^{A,link}\beta^{A}\left(m\Delta t^{B}\right)^{2}$$

Coupled solution on subdomain A

$$\ddot{\mathbf{u}}_{n+1}^{A} = \ddot{\mathbf{u}}_{n+1}^{A,\,free} + \ddot{\mathbf{u}}_{n+1}^{A,link}$$

$$\dot{\mathbf{u}}_{n+1}^{A} = \dot{\mathbf{u}}_{n+1}^{A,\,free} + \dot{\mathbf{u}}_{n+1}^{A,link}$$

$$\mathbf{u}_{n+1}^{A} = \mathbf{u}_{n+1}^{A,\,free} + \mathbf{u}_{n+1}^{A,link}$$

$$\dot{\mathbf{u}}_{n+\frac{j}{ss}}^{B,link} = \ddot{\mathbf{u}}_{n+\frac{j}{ss}}^{B,link}\gamma^{B}\Delta t^{B}$$

$$\mathbf{u}_{n+\frac{j}{ss}}^{B,link} = \ddot{\mathbf{u}}_{n+\frac{j}{ss}}^{B,link}\beta^{B}\Delta t^{B^{2}}$$

Coupled solution on subdomain B

$$\ddot{\mathbf{u}}_{n+\frac{j}{ss}}^{B} = \ddot{\mathbf{u}}_{n+\frac{j}{ss}}^{B,\,free} + \ddot{\mathbf{u}}_{n+\frac{j}{ss}}^{B,link}$$

$$\dot{\mathbf{u}}_{n+\frac{j}{ss}}^{B} = \dot{\mathbf{u}}_{n+\frac{j}{ss}}^{B,\,free} + \dot{\mathbf{u}}_{n+\frac{j}{ss}}^{B,link}$$

$$\mathbf{u}_{n+\frac{j}{ss}}^{B} = \mathbf{u}_{n+\frac{j}{ss}}^{B,\,free} + \mathbf{u}_{n+\frac{j}{ss}}^{B,link}$$

end

where,

$$\mathbf{D}_{m}^{A} = \mathbf{M}^{A} + \mathbf{C}^{A}\gamma^{A}m\Delta t^{A} + \mathbf{K}^{A}\beta^{A}\left(m\Delta t^{A}\right)^{2} \tag{4}$$

$$\mathbf{D}^{B} = \mathbf{M}^{B} + \mathbf{C}^{B}\gamma^{B}\Delta t^{B} + \mathbf{K}^{B}\beta^{B}(\Delta t^{B})^{2} \tag{5}$$

Since the PM method needs to be initialized, m is equal to 1 when n is equal to 0, and the PM method is equivalent to the GC method, which is a staggered procedure. After the initialization step, i.e. n > 0, m is equal to 2 and the two-step forward prediction allows for parallel implementations. For the purpose of HS, the restoring force of the PS $\mathbf{R}^{B}$is measured on physical specimens, after applying the trial displacement $\tilde{\mathbf{u}}_{n+\frac{j}{ss}}^{B,free}$. Moreover, based on previous equations, the Steklov-Poincare' operator $\mathbf{H}^{AB}$, can be quantified as follows:

$$\mathbf{L}^{A}\dot{\mathbf{u}}_{n+\frac{j}{ss}}^{A} + \mathbf{L}^{B}\dot{\mathbf{u}}_{n+\frac{j}{ss}}^{B} = \mathbf{L}^{A}\left(\dot{\mathbf{u}}_{n+\frac{j}{ss}}^{A,\,free} + \dot{\mathbf{u}}_{n+\frac{j}{ss}}^{A,link}\right) + \mathbf{L}^{B}\left(\dot{\mathbf{u}}_{n+\frac{j}{ss}}^{B,\,free} + \dot{\mathbf{u}}_{n+\frac{j}{ss}}^{B,link}\right) \tag{6}$$

$$\mathbf{L}^{A}\left(\dot{\mathbf{u}}_{n+\frac{j}{ss}}^{A,\,free}\right) + \mathbf{L}^{B}\left(\dot{\mathbf{u}}_{n+\frac{j}{ss}}^{B,\,free}\right) = \left(\mathbf{L}^{A}\mathbf{D}^{A^{-1}}\mathbf{L}^{A^{T}}\gamma^{A}\left(m\Delta t^{A}\right) + \mathbf{L}^{B}\mathbf{D}^{B^{-1}}\mathbf{L}^{B^{T}}\gamma^{B}\Delta t^{B}\right)\boldsymbol{\Lambda}_{n+\frac{j}{ss}} = \mathbf{H}^{AB}\boldsymbol{\Lambda}_{n+\frac{j}{ss}} \tag{7}$$

So, the $\Lambda_{n+\frac{j}{ss}}$ can be explicitly evaluated to cope with the synchronization requirements of HS. It is evident that the proposed method nicely suites the requirements of HS.

2.2 The modified PH method

The task sequence of the modified PH method [5] is sketched in Figure 2. As for the PM method, it clearly recalls the PH method [4]. However, the evaluation of the Lagrange multiplier vector Λ is done at the end of each macro time step Δt^A.

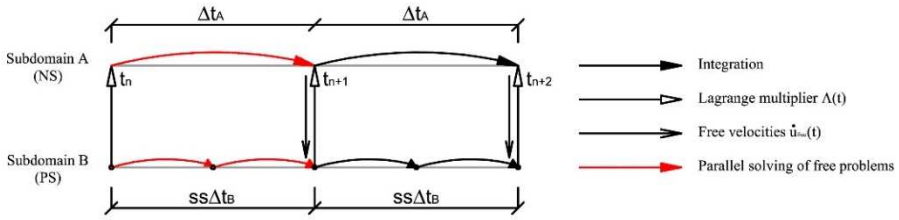

Fig. 2 - Task sequence of the modified PH method algorithm.

The red line describes the ongoing parallel process in the two subdomains. Note that the synchronized exchange of information enables the parallel computation of both subdomains. The modified PH method is briefly summarized herein.

Subdomain A

Solution of the free problem on subdomain A from $\boldsymbol{t_n}$ to $\boldsymbol{t_{n+1}}$

$$\tilde{\mathbf{u}}_{n+1}^{A,free} = \mathbf{u}_n^A + \dot{\mathbf{u}}_n^A \Delta t^A + \ddot{\mathbf{u}}_n^A \left(1/2 - \beta^A\right) \Delta t^{A^2}$$

$$\tilde{\dot{\mathbf{u}}}_{n+1}^{A,free} = \dot{\mathbf{u}}_n^A + \ddot{\mathbf{u}}_n^A \left(1 - \gamma^A\right) \Delta t^A$$

$$\ddot{\mathbf{u}}_{n+1}^{A,free} = \mathbf{D}^{A^{-1}} \left(\mathbf{F}_{n+1}^A - \mathbf{R}^A \left(\tilde{\mathbf{u}}_{n+1}^{A,free}, \tilde{\dot{\mathbf{u}}}_{n+1}^{A,free} \right) \right)$$

$$\dot{\mathbf{u}}_{n+1}^{A,free} = \tilde{\dot{\mathbf{u}}}_{n+1}^{A,free} + \ddot{\mathbf{u}}_{n+1}^{A,free} \gamma^A \Delta t^A$$

$$\mathbf{u}_{n+1}^{A,free} = \tilde{\mathbf{u}}_{n+1}^{A,free} + \ddot{\mathbf{u}}_{n+1}^{A,free} \beta^A \Delta t^{A^2}$$

Subdomain B

$$\mathbf{u}_n^{B,free} = \mathbf{u}_n^B, \dot{\mathbf{u}}_n^{B,free} = \dot{\mathbf{u}}_n^B$$

for j = 1:1:ss

Solution of the free problem on subdomain B from $\boldsymbol{t_n}$ to $\boldsymbol{t_{n+1}}$ in $\boldsymbol{ss}$ substeps

$$\tilde{\mathbf{u}}_{n+\frac{j}{ss}}^{B,free} = \mathbf{u}_{n+\frac{j-1}{ss}}^{B,free} + \dot{\mathbf{u}}_{n+\frac{j-1}{ss}}^{B,free} \Delta t^B + \ddot{\mathbf{u}}_{n+\frac{j-1}{ss}}^{B,free} \left(1/2 - \beta^B\right) \Delta t^{B^2}$$

$$\tilde{\dot{\mathbf{u}}}_{n+\frac{j}{ss}}^{B,free} = \dot{\mathbf{u}}_{n+\frac{j-1}{ss}}^{B,free} + \ddot{\mathbf{u}}_{n+\frac{j-1}{ss}}^{B,free} \left(1 - \gamma^B\right) \Delta t^B$$

$$\ddot{\mathbf{u}}_{n+\frac{j}{ss}}^{B,free} = \mathbf{D}^{B^{-1}} \left(\mathbf{F}_{n+\frac{j}{ss}}^A - \mathbf{R}^B \left(\tilde{\mathbf{u}}_{n+\frac{j}{ss}}^{B,free}, \tilde{\dot{\mathbf{u}}}_{n+\frac{j}{ss}}^{B,free} \right) \right)$$

$$\dot{\mathbf{u}}_{n+\frac{j}{ss}}^{B,free} = \tilde{\dot{\mathbf{u}}}_{n+\frac{j}{ss}}^{B,free} + \ddot{\mathbf{u}}_{n+\frac{j}{ss}}^{B,free} \gamma^B \Delta t^B$$

$$\mathbf{u}_{n+\frac{j}{ss}}^{B,free} = \tilde{\mathbf{u}}_{n+\frac{j}{ss}}^{B,free} + \ddot{\mathbf{u}}_{n+\frac{j}{ss}}^{B,free} \beta^B \Delta t^{B^2}$$

end

Calculation of interface Lagrange multipliers

$$\Lambda_{n+1} = \mathrm{H}^{AB^{-1}} \mathrm{V}_{n+1}$$

$$\mathbb{V}_{n+1}^A = \left[\ddot{\mathbf{u}}_{n+1}^{A,free^T} \quad \dot{\mathbf{u}}_{n+1}^{A,free^T} \quad \mathbf{u}_{n+1}^{A,free^T} \right]^T \qquad \mathbb{V}_{n+\frac{j}{ss}}^B = \left[\ddot{\mathbf{u}}_{n+\frac{j}{ss}}^{B,free^T} \quad \dot{\mathbf{u}}_{n+\frac{j}{ss}}^{B,free^T} \quad \mathbf{u}_{n+\frac{j}{ss}}^{B,free^T} \right]^T$$

$$\mathrm{V}_{n+1} = \left[\mathbb{V}_{n+\frac{1}{ss}}^{B^T} \quad \cdots \quad \mathbb{V}_{n+\frac{j}{ss}}^{B^T} \quad \cdots \quad \mathbb{V}_{n+1}^{B^T} \quad \mathbb{V}_{n+1}^{A^T} \right]^T$$

Calculation of link solutions

$$\mathrm{W}_{n+1} = \mathrm{Y}^{AB} \Lambda_{n+1}$$

$$\mathrm{W}_{n+1}=\left[\begin{array}{ccccccc}\mathbb{W}^{B^T}_{n+\frac{1}{ss}} & \cdots & \mathbb{W}^{B^T}_{n+\frac{j}{ss}} & \cdots & \mathbb{W}^{B^T}_{n+1} & \mathbb{W}^{A^T}_{n+1}\end{array}\right]^T$$

$$\mathbb{W}^{A}_{n+1}=\left[\begin{array}{ccc}\ddot{\mathbf{u}}^{A,link^T}_{n+1} & \dot{\mathbf{u}}^{A,link^T}_{n+1} & \mathbf{u}^{A,link^T}_{n+1}\end{array}\right]^T \quad \mathbb{W}^{B}_{n+\frac{j}{ss}}=\left[\begin{array}{ccc}\ddot{\mathbf{u}}^{B,link^T}_{n+\frac{j}{ss}} & \dot{\mathbf{u}}^{B,link^T}_{n+\frac{j}{ss}} & \mathbf{u}^{B,link^T}_{n+\frac{j}{ss}}\end{array}\right]^T$$

Calculation of the coupled solution

$$\mathrm{U}_{n+1}=\mathrm{V}_{n+1}+\mathrm{W}_{n+1}$$

$$\mathrm{U}_{n+1}=\left[\begin{array}{ccccccc}\mathbb{U}^{B^T}_{n+\frac{1}{ss}} & \cdots & \mathbb{U}^{B^T}_{n+\frac{j}{ss}} & \cdots & \mathbb{U}^{B^T}_{n+1} & \mathbb{U}^{A^T}_{n+1}\end{array}\right]^T$$

$$\mathbb{U}^{A}_{n+1}=\left[\begin{array}{ccc}\ddot{\mathbf{u}}^{A^T}_{n+1} & \dot{\mathbf{u}}^{A^T}_{n+1} & \mathbf{u}^{A^T}_{n+1}\end{array}\right]^T \quad \mathbb{U}^{B}_{n+\frac{j}{ss}}=\left[\begin{array}{ccc}\ddot{\mathbf{u}}^{B^T}_{n+\frac{j}{ss}} & \dot{\mathbf{u}}^{B^T}_{n+\frac{j}{ss}} & \mathbf{u}^{B^T}_{n+\frac{j}{ss}}\end{array}\right]^T$$

where,

$$\mathbf{D}^A=\mathbf{M}^A+\mathbf{C}^A\gamma^A\Delta^A_t+\mathbf{K}^A\beta^A\Delta t^{A^2} \tag{8}$$

$$\mathbf{D}^B=\mathbf{M}^B+\mathbf{C}^B\gamma^B\Delta^B_t+\mathbf{K}^B\beta^B\Delta t^{B^2} \tag{9}$$

Derivation of both coupling operators H^{AB} and Y^{AB} are briefly summarized. They can be easily derived on the linearized system of coupled equations (1-2) rearranged in matrix form. To this end, the Newmark algorithm is condensed to the following matrix equation,

$$\mathbb{M}^k\mathbb{U}^k_{n+1}=\mathbb{F}^k_{n+1}-\mathbb{N}^k\mathbb{U}^k_n \tag{10}$$

where,

$$\mathbb{M}^k=\left[\begin{array}{ccc}\mathbf{M}^k & \mathbf{0} & \mathbf{K}^k\\ -\gamma^k\Delta t^k\mathbf{I} & \mathbf{I} & \mathbf{0}\\ -\beta^k\Delta t^{k^2}\mathbf{I} & \mathbf{0} & \mathbf{I}\end{array}\right] \qquad \mathbb{N}^k=\left[\begin{array}{ccc}\mathbf{0} & \mathbf{0} & \mathbf{0}\\ -\left(1-\gamma^k\right)\Delta t^k\mathbf{I} & -\mathbf{I} & \mathbf{0}\\ -\left(1/2-\beta^k\right)\Delta t^{k^2}\mathbf{I} & -\Delta t^k\mathbf{I} & -\mathbf{I}\end{array}\right] \tag{11}$$

$$\mathbb{F}^k_{n+1}=\left[\begin{array}{c}\mathbf{F}^k_{n+1}\\ \mathbf{0}\\ \mathbf{0}\end{array}\right] \qquad \mathbb{U}^k_{n+1}=\left[\begin{array}{c}\ddot{\mathbf{u}}^k_{n+1}\\ \dot{\mathbf{u}}^k_{n+1}\\ \mathbf{u}^k_{n+1}\end{array}\right] \tag{12}$$

Accordingly, for a linearized system, the modified PH method can be expressed as,

$$\begin{bmatrix} \mathbb{M}^B & & & & & (1/ss)\mathbb{L}^B \\ \mathbb{N}^B & \mathbb{M}^B & & & & (2/ss)\mathbb{L}^B \\ & \ddots & \ddots & & & \vdots \\ & & \mathbb{N}^B & \mathbb{M}^B & & \mathbb{L}^B \\ & & & \mathbb{N}^B & \mathbb{M}^A & \mathbb{L}^A \\ & & & \mathbb{B}^B & \mathbb{B}^A & \mathbf{0} \end{bmatrix} \begin{bmatrix} \mathbb{U}^B_{n+\frac{1}{ss}} \\ \mathbb{U}^B_{n+\frac{2}{ss}} \\ \vdots \\ \mathbb{U}^B_{n+1} \\ \mathbb{U}^A_{n+1} \\ \mathbf{\Lambda}_{n+1} \end{bmatrix} = \begin{bmatrix} \mathbb{F}^B_{n+\frac{1}{ss}} - \mathbb{N}^B\mathbb{U}^B_n - (1-1/ss)\mathbb{L}^B\mathbf{\Lambda}_n \\ \mathbb{F}^B_{n+\frac{2}{ss}} - (1-2/ss)\mathbb{L}^B\mathbf{\Lambda}_n \\ \vdots \\ \mathbb{F}^B_{n+1} \\ \mathbb{F}^A_{n+1} - \mathbb{N}^A\mathbb{U}^A_n \\ \mathbf{0} \end{bmatrix} \tag{13}$$

Boolean matrices $\mathbb{L}^k$ and $\mathbb{B}^k$ localize Lagrange multipliers and coupling DoFs, respectively. Since the coupling of velocities was proved to favor the stability of the global scheme, they read,

$$\mathbb{L}^k = \begin{bmatrix} \mathbf{L}^{k^T} & \mathbf{0} & \mathbf{0} \end{bmatrix}^T, \quad \mathbb{B}^k = \begin{bmatrix} \mathbf{0} & \mathbf{L}^k & \mathbf{0} \end{bmatrix} \tag{14}$$

The linear system (13) can be solved using a bordered system approach. Subdomain matrix blocks can be gathered together and the system expressed as:

$$\begin{bmatrix} \mathrm{M} & \mathrm{L} \\ \mathrm{B} & 0 \end{bmatrix} \begin{bmatrix} \mathrm{U}_{n+1} \\ \Lambda_{n+1} \end{bmatrix} = \begin{bmatrix} \mathrm{F}_{n+1} \\ 0 \end{bmatrix} \tag{15}$$

Since the global solution is the sum of free and link quantities,

$$\mathrm{U}_{n+1} = \mathrm{V}_{n+1} + \mathrm{W}_{n+1} \tag{16}$$

where,

$$\mathrm{V}_{n+1} = \mathrm{M}^{-1}\mathrm{F}_{n+1} \tag{17}$$

$$\mathrm{W}_{n+1} = -\mathrm{M}^{-1}\mathrm{L}\Lambda_{n+1} = \mathrm{Y}^{AB}\Lambda_{n+1} \tag{18}$$

The second block row of (24) can be split as follows,

$$\mathrm{B}\mathrm{U}_{n+1} = \mathrm{B}\mathrm{V}_{n+1} + \mathrm{B}\mathrm{W}_{n+1} = 0 \tag{19}$$

Accordingly, Lagrange multipliers λ_{n+1} can be easily expressed through the Steklov-Poincaré operator H^{AB}, which is the dual Shur complement of the block matrix reported in (15),

$$\Lambda_{n+1} = -\left(\mathrm{B}\mathrm{M}^{-1}\mathrm{L}\right)^{-1}\mathrm{B}\mathrm{V}_{n+1} = \mathrm{H}^{AB^{-1}}\mathrm{V}_{n+1} \tag{20}$$

In this way, the relevant energy at the interface is preserved.

3 THE RIO TORTO BRIDGE CASE STUDY

The Rio Torto viaduct is a RC structure built during the sixties and located between Florence and Bologna in Italy. Twelve portal piers support the thirteen-span bay deck of each independent roadway as shown in Figure 3. End spans measure 29 m, whilst internal spans 33 m. Six Gerber saddles are present in the middle of the bridge and close to both abutments. Additional details can be found in [8, 9].

Fig. 3. Lateral view of the Rio Torto viaduct.

Solid and hollow circular cross section columns characterize short and tall piers, respectively. Relevant diameters measure 1200 mm and 1600 mm. The taller Pier #7 measured 41.34 m, whilst the shorter Pier #12 measured 13.80 m. Gerber saddles were removed in the isolated configuration where a pair of Concave Sliding Bearing (CSB) isolator were interposed between the deck and each pier. A comprehensive set of time history analyses of a refined FE model of the bridge was conducted in the OpenSees environment at both the SLS and ULS. With reference to the *as built* configuration, all piers showed hysteretic dissipation already at SLS. Conversely, time history analyses conducted in the *isolated* case proved that isolator pairs dissipated the most of hysteretic energy whilst piers remained in the linear range. A linear response of the deck was observed for both conditions. Moreover, numerical simulations highlighted that frame piers experienced in-plane deformations. In order to comply with the computational and control performance of the experimental facility for complex HSs, a reduced 88-DoFs substructured model of the viaduct was assembled for the *as built* and the *isolated* case [8, 9].In greater detail, the internal constraint setting was simplified and out-of-plane displacements of piers were fixed, whilst relative rotations among the deck and piers were released. Figure 4 depicts schematics of bridge configuration with node numbering, dimensions and frequencies of the four lowest eigenmodes. Nonlinear reduced S-DoF piers, provided transversal stiffness to the deck, whose cross sectional characteristics were $A = 4.63\ m^2, Ixx = 51.90\ m^4, Izz = 3.45\ m^4, Iyy = 0.10\ m^4$.

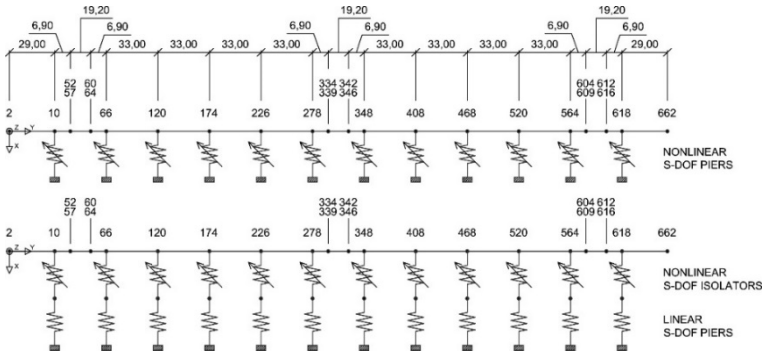

a

Mode	Freq. [Hz]
1	0.3674
2	0.3771
3	0.3922
4	0.4607

b

Mode	Freq. [Hz]
1	0.5010
2	0.6606
3	0.9392
4	1.3642

Fig. 4. Plan view of the reduced nonlinear models of the Rio Torto viaduct in: a) as built configuration; b) Isolated configuration. Dimensions in m;

As can be appreciated from Figure 4, Pier #9 and #11 were substructured in the laboratory together with related pairs of CSB isolators. The deck, remaining piers and related isolators were simulated numerically by means of reduced state space models. In greater detail, nonlinear S-DoF reduced models of piers were based on a modified version of the well-known Bouc-Wen mode. They were capable of reproducing the softening behavior predicted by the aforementioned refined OpenSees FE model. To this end, the factor $1/(1 + \alpha x^2)$ was added to modify the linear component of the tangent stiffness and a ρ parameter was introduced to simulate the degradation of the linear stiffness k. The resulting formulation reads,

$$\begin{cases} r + c \cdot \dot{x} + m \cdot \ddot{x} = -f \cdot \ddot{u}_g(t) + p(t) \\ \dot{r} = \left[\rho \cdot k / \left(1 + \alpha \cdot x^2\right) - (\beta \cdot sgn(\dot{x} \cdot r) + \gamma) \, | r |^n \right] \cdot \dot{x} \end{cases} \tag{21}$$

where β, γ and n are parameters of the Bouc-Wen model. In order to decrease the number of nonlinear parameters, γ and n were set to zero and to one, respectively [10]. Because, reduced nonlinear springs were not capable of reproducing piers' behavior at their full operating range, a set of parameters was identified for each different limit state. In order to force a linear response of piers without damage, β and ρ were set to zero, respectively, in the *isolated* case. Single Friction Pendulum Bearing OpenSees elements embed a physical model that is able to replicates the slip mechanism of CSB devices. Because bilinear shapes characterize inherent hysteretic loops, the state space model proposed by [11] was selected to reproduce the NS of isolator elements. Although the effect of variable vertical loads was neglected in the NSs, simplified bilinear hysteretic models well reproduced the response of all OpenSees isolators. Identified values of all nonlinear parameters of both reduced isolators and piers can be found in [8, 9].

4 NUMERICAL COMPARISON OF PROPOSED METHODS

In the following, the algorithmic performance of the aforementioned algorithm are compared in a pure numerical setting. From the HS perspective, the behavior of link solutions is crucial. In fact, their magnitude directly reflects on smoothness of actuators trajectories. Along this line, the following analyses try to shed light on both link quantities, which force velocity continuity at the interface between the NS and PS. Figure 5 depicts a schematic of the isolated bridge model with particular emphasis to the substructuring scheme.

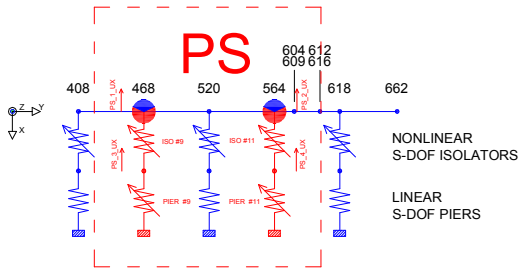

Fig. 5. Close up view on the substructuring scheme of the reduced nonlinear models of the Rio Torto viaduct in the Isolated configuration.

As can be appreciated from Figure 5, both interface Nodes #468 and #564 gather mass from both the deck and the related CSB isolator element. The last contributions is very small and entails high frequency eigenmodes on each 2-DoFs PS when detached from the overall bridge, i.e. in the decoupled configuration, hereinafter. In principle, resulting faster dynamics increase free displacements $\mathbf{u}^B_{free}$ on the physical side, and therefore, that link displacements $\mathbf{u}^B_{link}$ must compensate for within the subcycling time. As a consequence, actuators, which span free solutions, can potentially experience sharp trajectories that reduce the quality of the test. In order to mitigate such effect, part of the mass on the deck side -NS- is moved on the isolator side -PS-. Since both contributions share the same nodes, the overall dynamics remains unchanged and eigenfrequencies of the decoupled PS are pleasantly reduced. As a result, the PS benefits of smaller link displacements $\mathbf{u}^B_{link}$, and therefore, actuators experience smoother

trajectories. The mass fraction parameters m_f was introduced to modulate the mass transfer among NSs and PSs as follows,

$$\mathbf{M}_i^{B'} = \mathbf{M}_i^B + m_f \cdot \mathbf{M}_i^A, \mathbf{M}_i^{A'} = \left(1 - m_f\right) \cdot \mathbf{M}_i^A \tag{22}$$

where the subscript i stands for interface; accordingly, mass matrices of (22) must be intended confined to interface DoFs. Therefore, $\mathbf{M}^{A'}$ and $\mathbf{M}^{B'}$ matrices characterize the interface DoFs masses of the PS and the NS, respectively, during HS. For the sake of clarity, Table 2 summarizes the eigenfrequencies of the decoupled 4-DoFs PS for different values of the mass fraction parameter.

Table 2 - Eigenfrequency of the decoupled PS

	Mass fraction m_f			
Mode	0.001	0.005	0.05	0.95
1	2.36	2.32	1.96	0.76
2	3.56	3.50	2.98	1.15
3	135.82	61.81	23.03	13.69
4	174.67	79.45	29.53	17.51

As can be appreciated from Table 2, a very small contribution of 0.005 already halves isolator eigenfrequencies. Clearly, such high frequency modes are not present in the PS of the as built configuration. Therefore, the isolated bridge is considered to compare algorithmic performance. In this preliminary study, coarse time step quantities are analyzed. Future investigations will shed light also on subcycling solutions. The same coarse time step was considered for both algorithms, i.e. $\Delta t^A = 1/1024s$. Moreover, a Newmark implicit scheme - $\gamma = 0.5$ and $\beta = 0.25$ - was applied to both subdomains. In order to estimate errors, a reference solution was calculated considering a monolithic implementation of the Newmark implicit scheme with a time integration step $\Delta t = \Delta t^A/100$. All reported results refer to the transversal displacement DoF of Node #468, which connects Pier #9 and related isolator to the deck. In detail, Figures 8 and 10 compares link displacement histories obtained from both the PM and the modified PH methods for different subcycling and mass fraction setting.

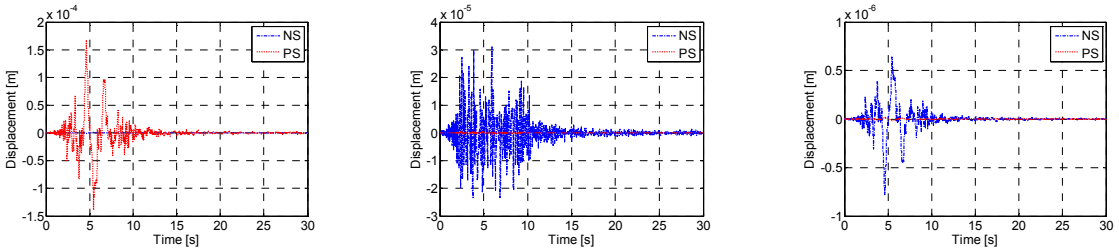

a) b) c)

Fig.6 - PM method: link displacement solutions in the case of: a) $\boldsymbol{ss = 1, m_f = 0.001}$; b) $\boldsymbol{ss = 1, m_f = 0.95}$; and c) $\boldsymbol{ss = 100, m_f = 0.001}$.

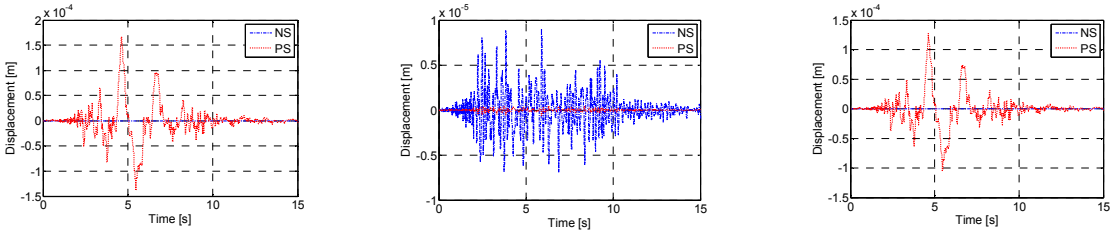

a) b) c)

Fig. 7 - Modified PH method: link displacement solutions in the case of: a) $\boldsymbol{ss = 1, m_f = 0.001}$; b) $\boldsymbol{ss = 1, m_f = 0.95}$; and c) $\boldsymbol{ss = 100, m_f = 0.001}$.

As can be appreciated from Figures 6a, 6b, 7a and 7b, given the same subcycling ss the mass fraction parameter affects $link$ displacements that prevail where the mass is smaller, and both the PM and the modified PH algorithms show the same behavior. Conversely, as can be observed in Figures 6c and 7c, only the PM method can benefit of subcycling for reducing $link$ displacements on the PS.

5 THE EXPERIMENTAL FRAMEWORK FOR HYBRID SIMULATION

A comprehensive set of HSs of the viaduct was conceived. The PM method was selected as parallel partitioned time integrator. Its inherent subcycling capabilities permit the synchronization of the two separated integration processes that involve both NSs and PSs with a coarse time step Δt_A and a fine Δt_B and, respectively. As a result, smooth actuator trajectories were achieved. In this particular case, an extended time scale $\lambda = 200$ was assumed together with a subcycling parameter ss equal to 250. As result, $\Delta t_A = 2.5$ ms was applied to NSs, whilst $\Delta t_B = 0.01$ ms was selected for PSs. Thus, actuator displacement commands were generated on the PS at the controller rate of 500 Hz. An additional computational driver ran the Cast3m FE model of the NS. 2.5 scale mock-up models of Piers #9 and #11 were experimentally substructured in the ELSA laboratory. Since gravity loads did not play an important role on piers, Procedure #2 proposed by [12] was selected for specimen scaling. Therefore, scale factors S and S^2 were applied to displacements and forces, respectively. Hence, both stress and strain quantities were preserved. Several HSs were carried out. Figure 8 depicts the experimental setup and the hysteretic response of Pier #9 during Test k09 and Test l02, which correspond to the as built and the isolated configuration at ULS, respectively.

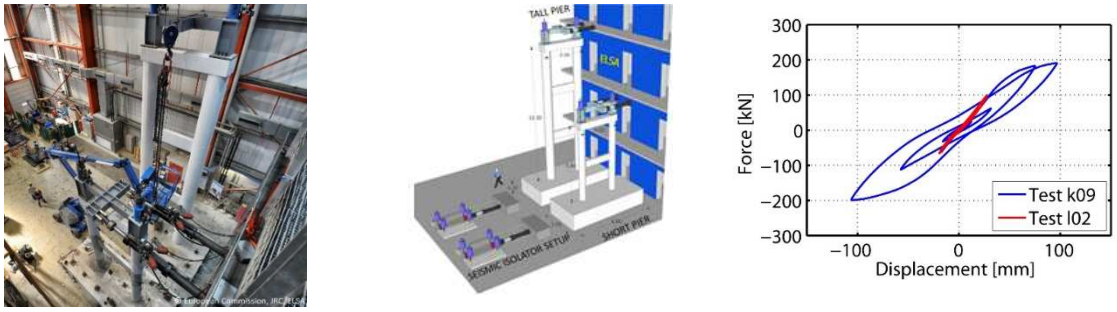

a) b) c)

Fig. 8. a) 1:2.5 mock-up scale specimens of Piers #9 and #11; b) vertical loading system of frame piers. c) Comparison of hysteretic loops of HS k09 and l02, i.e. as-built and isolated configurations at ULS, respectively, for Pier #9

As can be appreciated from Figure 8c, HSs proved the effectiveness of the retrofitting scheme based on CSB isolators.

6 CONCLUSIONS

Mixed implicit/explicit multi-time partitioning methods are ripe for a profitable application to HS. From this perspective, the present paper presents a preliminary study on the performance of the PM and modified PH methods tailored to hybrid systems. A twelve-pier reinforced concrete was introduced as reference case study. Comparisons were done in term of link displacement quantities, which must entail smooth actuator trajectories. During HS umerical

simulations and experimental tests proved that both algorithms are suitable to HS. In this respect particular care must be devoted to the partitioning of mass between PS and NS. Future investigation will be addressed in the frequency domain, where spectral distributions of errors, kinematic quantities and Lagrange multipliers can be compared to eigenfrequencies of both coupled and decoupled substructures.

7 ACKNOWLEDGMENTS

The financial support from the SERIES (Seismic Engineering Research Infrastructures for European Synergies) Project, funded within the 7th Framework Programme of the European Commission [FP7/2007-2013] under grant agreement n° 227887, is greatly appreciated. Any opinions, findings and conclusions or recommendations expressed in this paper are those of the authors and do not necessarily reflect those of SERIES sponsors.

REFERENCES

[1] Pegon P. Continuous PsD Testing With Substructuring. In O. S. Bursi and D. J. Wagg, editors, Modern Testing Techniques for Structural Systems, Dynamics and Control. CISM-Springer Wien NewYork, 2008.

[2] A. Gravouil, A. Combescure . Multi-time-step explicit – implicit method for non-linear structural dynamics, pp 199–225, 2001.

[3] P. Pegon and G. Magonette Continuous PSD testing with nonlinear substructuring: presentation of a stable parallel inter-field procedure. Technical Report 1.02.167, E.C., JRC, ELSA, Ispra, Italy, 2002.

[4] Brun, M., Batti, a., Combescure, a., & Gravouil, a. (2014). External coupling software based on macro- and micro-time scales for explicit/implicit multi-time-step co-computations in structural dynamics. Finite Elements in Analysis and Design, 86, 101–119. doi:10.1016/j.finel.2014.04.005.

[5] A. Prakash, K. D. Hjelmstad. A FETI-based multi-time-step coupling method for Newmark schemes in structural dynamics. International Journal for Numerical Methods in Engineering, 61(13), pp 2183–2204, 2004.

[6] Newmark, N. M. (1959) A method of computation for structural dynamics. Journal of Engineering Mechanics, ASCE, 85 (EM3) 67-94.

[7] A. Bonelli, O.S. Bursi, L. He, G. Magonette, P. Pegon. Convergence analysis of a parallel interfield method for heterogeneous simulations with dynamic substructuring. International Journal for Numerical Methods in Engineering, 75(7), pp 800–825, 2008.

[8] Abbiati G., Bursi O.S., Caperan P., Di Sarno L., Molina F.J., Paolacci F., Pegon P., 2014. Hybrid simulations of a multi-span RC viaduct with plain bars and sliding bearings. Earthquake Engineering and Structural Dynamics – under review

[9] Paolacci, F. et al. 3-D Assessment of the seismic vulnerability of an old RC viaduct with frame piers and study of the effectiveness of base isolation through PsD testing (RETRO), Eur Report 26471 EN , 2014. JRC., European Union.

[10] Abbiati G. Dynamic Substructuring of Complex Hybrid Systems Based on Time-Integration, Model Reduction and Model Identification Techniques", PhD Thesis, Department of Civil, Env. & Mechanical Engineering, University of Trento, 2014.

[11] Mostaghel, N. Analytical Description of Pinching, Degrading Hysteretic Systems. Journal of Engineering Mechanics, 1999, 2:125, 216-224.

[12] Kumar, S., Itoh, Y., Saizuka, K., and Usami, T. Pseudodynamic Testing of Scaled Models. Journal of Structural Engineering, 1997, 123(4), 524–526.